Development and Preliminary Validation of an Efficient Alkali Metal Heat Pipe Analysis Model for Long Time Transient Simulations*

Chuntao Tang,[1] Kang Chen,[1, †] Kaiyuan Zhu,[2] Guojun Hu,[2, ‡] Qichang Chen,[1] Chang Zhang,[1] Jinkun Zhao,[1] and Botong Dong[1]

[1]*Shanghai Nuclear Engineering Research & Design Institute CO., LTD.*

[2]*School of Nuclear Science and Technology, University of Science and Technology of China, Hefei Anhui, China*

Heat pipe cooled reactors are ideal for space power, military, and marine energy applications. A key aspect in the safety analysis of the heat pipe cooled reactor is the efficient modeling of heat pipes and their coupling with the solid reactor core. When a heat pipe begins in a cold state, the working substance within the vapor core transitions through several stages, moving from rarefied vapor flow to continuous vapor flow. This progression complicates the analysis of transient heat pipe behaviors. This work aims to develop a core analysis model for the heat pipe cooled reactor based on the coupling of ANSYS/Fluent and a newly developed transient heat pipe analysis code HePIRE-HA. A compressible two-equation model for the heat pipe vapor core is developed and solved alongside the heat pipe wall and wick through a fully-implicit solution scheme. A comprehensive interface tracking scheme has been developed to effectively manage the transition from a rarefied vapor state to a continuous vapor state. This transition scheme is demonstrated to work reasonably well and shows great efficiency. The coupling of ANSYS/Fluent and HePIRE-HA is achieved through the User Defined Function (UDF) capability of ANSYS/Fluent. A series of verification and validation studies is conducted to assess the performance and capabilities of the newly developed model. The results highlight that the new coupling model effectively predicts the transient response of the reactor core, making it a trustworthy tool for designing and ensuring the safety of the heat pipe cooled reactor.

Keywords: Heat Pipe; Micro Reactor; RETA; ANSYS.

I. INTRODUCTION

A heat pipe reactor, classified as a solid-state reactor, does not utilize a primary coolant loop to facilitate the transfer of heat from the core. Instead, it uses heat pipes to passively transfer heat from the core. This design confers numerous advantages for heat pipe cooled reactors, including ease of operation, miniaturization, and reliability[1]. Heat pipe reactors offer reliable nuclear energy for deep space exploration, remote areas, marine power, and floating platforms[2, 3].

A heat pipe is composed of the wall, working substance, and wick. It has very high thermal conductivity, allowing it to maintain an almost uniform temperature along its heated and cooled sections[4]. In practical applications, the frozen start-up processes of a heat pipe involve intricate physical phenomena, including two-phase flow, phase change, and porous media flow[5]. These factors pose challenges for analyzing heat pipe reactors. Calculating and analyzing heat pipes are essential for the thermal design and safety evaluation of heat pipe reactors.

The heat pipe model can be divided into three types based on the modeling method of vapor flow in the vapor core: thermal resistance method[6], single-phase flow method[7], and two-phase flow method[8]. Among them, the thermal resistance method[6] considers heat pipes as a heat resistance network. This method has poor accuracy, and it is difficult to simulate the vapor flow state in heat pipes. The two-phase

flow method[8] is immature; the convergency issue makes it difficult to simulate the frozen startup processes of heat pipes. The single-phase flow model captures vapor flow characteristics effectively and converges better than the two-phase flow model. At present, the single-phase flow model[7] typically simulates the frozen startup of the heat pipe by determining the transition temperature of the continuum flow state; the rarefied vapor flow is typically ignored during the initial startup of the heat pipe.

This work will propose a new vapor flow model. In this new model, during the heat pipe's frozen startup, the vapor density in the core increases until reaching a steady state, undergoing three stages: vacuum, transition vapor flow, and continuum flow. The cylindrical heat pipe's angular symmetry allows for a two-dimensional modeling approach[9]. In this way, we can accurately and quickly simulate the frozen startup of a heat pipe. This new model and the heat pipe analysis code HePIRE-HA are developed on top of the generic code framework RETA[10].

The modeling of solid-state reactor cores can be divided into three types[11]: multi-channel one-dimensional models[12, 13], multi-channel two-dimensional models[14], and three-dimensional models[15]. The multi-channel and one-dimensional models are well suited for system-level safety analysis but compromise for computational accuracy [16–18]. In the contrast, the three-dimensional reactor core model is the most accurate but asks for the most computational resources. The primary objective of these work is the multi-physics simulations of the heat pipe reactors, and much progress has been made [19–24]. For example, Guo et al.[25] applied the lumped parameter method for modeling heat pipes in their heat pipe reactor simulations and utilized OpenFOAM to simulate the three-dimensional core. Lee et al.[26] utilized ANSYS to create a three-dimensional model of heat pipes and

† Corresponding author, chenkang1@snerdi.com.cn.

‡ Corresponding author, huguojun@ustc.edu.cn.

cores, allowing for a monolithic solution for the heat pipe reactor. As heat pipes are modeled in two dimensions, the vapor flow control equation differs from the heat conduction control equation for the core. Generally, the core section takes longer to resolve than the heat pipe section. The heat conduction equation is simpler to solve than the vapor flow equation. Consequently, this paper employs the iterative method to analyze the coupling between the core and heat pipes.

This article is organized as follows: Section II introduces physics models and numerical solution framework of the heat pipe code HePIRE-HA; Section III presents the verification and validation of the heat pipe and coupling models; Section IV uses the developed heat pipe reactor thermal analysis program to conduct steady-state and transient thermal analysis of the KRUSTY reactor[27]; Section V discusses conclusions and future prospects.

II. MODEL DESCRIPTION

A. Heat pipe model

The study considers the conventional cylindrical heat pipes, which are composed of the heat pipe wall, wick, and vapor core regions. This work considers the compressible one-dimensional flow model for the vapor core. The one-dimensional vapor flow model will be coupled with a cylindrical two-dimensional heat conduction model for the heat pipe wall and wick. The explicit coupling between the wick and vapor core is avoided by coupling them internally in this newly developed model.

As shown in Fig. 1, the startup process of a heat pipe[28] from a cold state can be divided into the following five stages:

1. When the heat pipe starts, the working substance in the wick is solid. The vapor core can be considered a vacuum.

2. As heat continuously flows into the evaporator section of the heat pipe, the working substance in the wick begins to melt. Since the solid-liquid interface has not yet reached the interface between the wick and the vapor core, there is no evaporation, and the vapor core remains in a vacuum state.

3. In the evaporator section, the working substance in the wick completely melts, and the fluid evaporates at the gas-liquid interface. At this time, the vapor pressure is very low, and the vapor core is in a state of rarefied vapor or transition vapor flow. In the adiabatic section and the condenser section, part of the working substance in the wick is still in a solid state.

4. As the evaporation process continues, the vapor accumulated in the vapor core becomes sufficient, and continuum vapor flow begins from the evaporator section. Near the end of the condenser section, the vapor flow is still in a state of rarefied vapor or transition vapor flow, and the vapor core as a whole is in a transitional state.

5. The working substance in the wick completely melts, and the vapor core is entirely in a state of continuum vapor flow until it reaches a steady state.
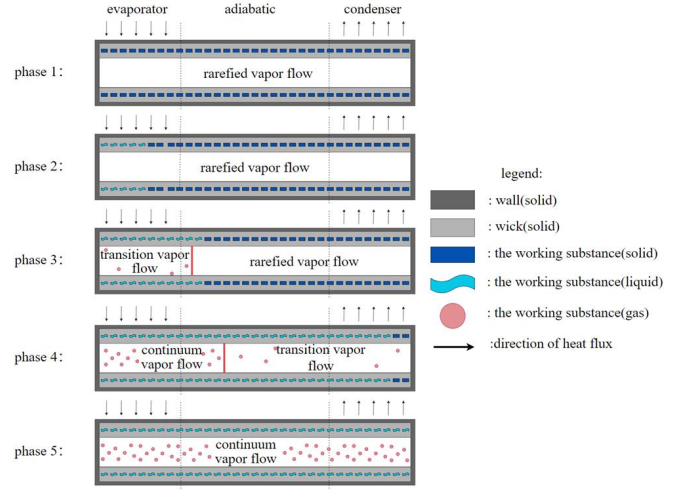

Fig. 1. Illustration of the startup process of a heat pipe from a frozen state.

The state of the working substance in the core region depends mainly on the density (and thus the temperature) of the vapor during the startup process. The dimensionless Knudsen number (Kn), defined as the ratio of the molecular mean free path length to the vapor core diameter, is commonly used to determine the different phases of the vapor core. In this work, the vapor flow is identified as rarefied vapor flow when Kn is larger than 10 and as continuum vapor flow when Kn is smaller than 0.01. For the case $0.01 \leq Kn \leq 10$, the vapor flow could be a mixture of rarefied vapor flow, transition vapor flow, and continuum vapor flow. In the practical implementation, the transition Knudsen number is converted to a transition temperature T^* using the kinetic theory of gases as follows:

$$\rho\left(T^*\right) = \frac{1.051\kappa}{\sqrt{2}\pi\sigma^2 RD \cdot \text{Kn}} \quad (1)$$

In which, ρ is the density of vapor, κ is the Boltzmann constant in the unit of J/K, σ is the Stefan-Boltzmann constant in the unit of W/(m^2 K^4), R is the gas constant in the unit of J/(kg K), and D is the diameter of vapor core in the unit of m. Note that the transition temperature T^* may need to be solved iteratively using Equation (1) when the vapor Equation of State (EOS) is complex.

1. Heat pipe wall and wick model

The heat pipe wall and wick regions are modeled as a two-dimensional axisymmetric solid heat structure. The governing equation for solid temperature is

$$\rho_s c_{p,s}\frac{\partial T_s}{\partial t} - \frac{1}{r}\frac{\partial}{\partial r}\left(rk_s\frac{\partial T_s}{\partial r}\right) - \frac{\partial}{\partial z}\left(k_s\frac{\partial T_s}{\partial z}\right) - q_s''' = 0 \quad (2)$$

In which subscript s represents solid. Note that solid density ρ_s, specific heat capacity $c_{p,s}$, and thermal conductivity k_s are all temperature-dependent. The nonlinearity due to this dependency is resolved by the fully-implicit solution scheme.

Given the high thermal conductivity of the liquid metal working substance and the thin wick thickness, the influence of liquid flow in the wick can be disregarded without introducing notable errors in the macroscopic average temperature of the wick structure[13]. We will disregard the liquid flow in the wick structure and treat it as a solid region for heat conduction. The effective thermal conductivity will be assessed considering the wick structure's porosity, the thermal conductivity of the fluid, and the conductivity of the wick material. During the cold startup of the heat pipe, the effective properties of the wick structure are largely influenced by the wick's temperature, as this affects the melting of the working materials. In this work, the effective properties of wick structure are formulated as:

$$k_{s,\,\text{wick}}(T) = \begin{cases} k_{se} & T < T_m - \delta T \\ k_{se} + (k_{le} - k_{se})\frac{T - T_m + \delta T}{2\delta T} & T_m - \delta T \leq T \leq \delta T + T_m \\ k_{le} & T > T_m + \delta T \end{cases} \tag{3}$$

In which T_m is the melting temperature of the working substance and δT is a controllable temperature interval. The effective thermal conductivity of the wick structure is transitioned from k_{se} to k_{le} when the wick temperature increases across the melting temperature. k_{se} and k_{le} is the effective thermal conductivity of the wick when the working substance is in the solid state and liquid state, respectively. This work focuses on the wrapped screen wick design where the effective thermal conductivity is affected by the porosity (φ):

$$k_{Se} = \frac{k_1\left[(k_1 + k_{SW}) - (1 - \varphi)(k_1 - k_{SW})\right]}{\left[(k_1 + k_{SW}) + (1 - \varphi)(k_1 - k_{SW})\right]} \tag{4}$$

$$k_{le} = \frac{k_2\left[(k_2 + k_{SW}) - (1 - \varphi)(k_2 - k_{SW})\right]}{\left[(k_2 + k_{SW}) + (1 - \varphi)(k_2 - k_{SW})\right]} \tag{5}$$

In which k_1 and k_2 are the thermal conductivity of working substance in pure solid and liquid state, and k_{sw} is the thermal conductivity of screen material. Similarly, the effective heat capacity of the wick structure is

$$(\rho c_p)_{s,\,\text{wick}} = \varphi(\rho c_p)_2 + (1 - \varphi)(\rho c_p)_{ws} \tag{6}$$

In which $(\rho c_p)_2$ is the heat capacity of the working substance in a liquid state.

2. Continuum vapor flow model

A two-equation vapor flow model is employed when the vapor exists in a continuum state. Assuming the vapor flow is in saturation condition, the conservation equations for the vapor flow are formulated using the mass and momentum equation as,

$$\frac{\partial \rho}{\partial t} + \frac{\partial \rho u}{\partial z} - \Gamma = 0 \tag{7}$$

$$\frac{\partial \rho u}{\partial t} + \frac{\partial \rho u^2}{\partial z} + \frac{\partial p}{\partial z} + \frac{\lambda}{2D_h}\rho u|u| = 0 \tag{8}$$

In which Γ is the mass generation rate per unit volume, D_h is the hydraulic diameter of the vapor core region, and λ is the dimensionless friction coefficient.

The heat pipe vapor core is coupled with the wick's inner surface through a convection-like formula. A user-specified effective heat transfer coefficient h_v is used to couple the vapor core temperature T and solid temperature T_s by

$$q_s'' = -k_s\frac{\partial T_s}{\partial r} = h_v(T_s - T) \tag{9}$$

In which q_s'' is the heat flux at the wick-core interface. For the heat pipe, the heat transfer at the wick-core interface is, in fact, through the evaporation/condensation of the working substance. The mass generation rate Γ is computed from the heat flux by

$$\Gamma = \frac{a_w q_s''}{h_{fg}} \tag{10}$$

In which a_w is the heat transfer surface area density per unit volume and h_{fg} is the latent heat of evaporation/condensation.

This work considers mainly high-temperature alkali metal heat pipes with Sodium or Potassium as the working substance. Let T and p be the vapor temperature and pressure. The EOS of the vapor core material is modeled by a group of 5th-order polynomials, where the thermodynamic and mechanical properties of vapor are formulated as functions of the saturation temperature by

$$\begin{cases} \text{for density: } \ln(\phi) = \sum_{m=0}^{5} A_m T_v^m \\ \text{for other properties: } \phi = \sum_{m=0}^{5} A_m T_v^m \end{cases} \tag{11}$$

In which ϕ represents a thermodynamic or mechanical property of the vapor. The coefficients A_m for the Sodium [30] and Potassium [31] are listed in Table 1 for reference.

In the current formulation, the vapor is assumed to be in the saturated condition, and the Clausius-Clapeyron equation is used to determine the vapor saturation temperature from the vapor pressure,

Table 1. Coefficients of fitting polynomials for Sodium and Potassium.

	Properties	A_0	A_1	A_2	A_3	A_4	A_5
Sodium:371K-1800K	Pressure	-5.73e+03	1.81e+01	-2.25e-02	1.52e-05	-5.30e-09	7.50e-13
	Density	-5.76e-02	1.82e-04	-2.29e-07	1.56e-10	-5.51e-14	7.86e-18
	Heat capacity	-9.50e+03	3.49e+01	-3.25e-02	8.57e-06	2.28e-09	-1.03e-12
	Heat conductivity	8.88e-02	-4.50e-04	1.12e-06	-1.04e-09	4.41e-13	-7.12e-17
	Viscosity	6.54e-06	1.27e-08	-3.93e-12	1.52e-14	-1.08e-17	2.36e-21
Potassium:600K-1500K	Pressure	-6.08e+06	2.01e+04	-2.96e+01	-2.39e-02	-1.00e-5	1.71e-9
	Density	-4.39e-02	1.51e-04	-1.99e-07	1.45e-10	-5.60e-14	8.86e-18
	Heat capacity	1.11e+02	-8.17e-01	2.65e-03	-3.15e-06	1.63e-09	-3.15e-13
	Heat conductivity	6.09e-02	-3.49e-04	8.01e-07	-7.97e-10	3.77e-13	-6.92e-17
	Viscosity	-8.41e-06	6.35e-08	-8.34e-11	5.98e-14	-1.52e-17	1.28e-32

$$\frac{dp}{p} = \frac{h_{fg}}{R}\frac{dT}{T^2} \tag{12}$$

In which h_{fg} is the specific enthalpy of vaporization. In practice, given the reference temperature T_c and reference pressure p_c, the saturation temperature is derived as

$$\frac{1}{T} = \frac{1}{T_c} - \frac{R}{h_{fg}}\ln\frac{p}{p_c} \tag{13}$$

Using the Clausius-Clapeyron equation, the pressure gradient term in Equation (8) is transformed into

$$\frac{\partial p}{\partial z} = \frac{dp}{dT}\frac{\partial T}{\partial z} = \frac{\rho h_{fg}}{T}\frac{\partial T}{\partial z} \tag{14}$$

With vapor temperature as the dependent variable, the vapor density is formulated as

$$\rho = \frac{p_c}{RT}\exp\left[\frac{h_{fg}}{R}\left(\frac{1}{T_c} - \frac{1}{T}\right)\right] \tag{15}$$

A closed-form friction coefficient correlation is required to correctly predict the flow field in the vapor core region. The friction coefficient λ in Equation (8) depends on the Reynolds number. In this study, the friction coefficient is modeled as

$$\lambda = \begin{cases} \frac{64}{\text{Re}} & \text{Re} \le 2200 \\ 0.0291 + 1.7\times 10^{-5}(\text{Re} - 2200) & 2200 < \text{Re} < 3000 \\ \frac{0.316}{\text{Re}^{0.25}} & \text{Re} > 3000 \end{cases} \tag{16}$$

B. Rarefied vapor flow model

The density of vapor in the Rarefied state is quite small, and heat transfer through Rarefied vapor flow is negligible. In this work, the Rarefied vapor flow region is treated as a vacuum region. In the practical implementation, the vapor velocity at the Rarefied transition boundary is set to zero. When the heat pipe temperature rises, the Rarefied transition boundary moves smoothly along the heat flow direction until it reaches the condenser end.

1. Transition vapor flow model

When the flow in the vapor core is in the Transition vapor state, the vapor density and mass flux are not negligible. The heat flux brought by the Transition vapor flow helps heat up the remaining cold region. For simplicity, a diffusion model is used in this work to model the Transition vapor flow, i.e.

$$\frac{\partial \rho}{\partial t} - \frac{\partial}{\partial z}\left(D_K\frac{\partial \rho}{\partial z}\right) - \Gamma = 0 \tag{17}$$

In which Γ is the mass generation rate per unit volume. In which D_K is the diffusion coefficient[29] of the vapor calculated by

$$D_K = \frac{2R_v}{3}\bar{v} = \frac{2R_v}{3}\sqrt{\frac{8\kappa T}{\pi m_g}} \tag{18}$$

In which R_v is the radius of the vapor core, $\bar{v}$ is the average molecular speed, and m_g is the molecular mass of the vapor.

2. Heat pipe boundary conditions

Flexible boundary conditions are available for the heat pipe evaporator and condenser outer wall, including temperature, heat flux, convection, and radiation boundary conditions. At both ends of the heat pipe, the velocity and temperature gradient of vapor flow are set to zero. During the startup stage, the mass flux at the boundary of different vapor flow regions is set according to the flow conditions. At the Rarefied-Transition boundary, the mass flux is set to zero; at the Transition-Continuum boundary, the mass flux is set to the diffusive

flux(ρu).

C. Heat pipe solution method

The heat pipe model has been integrated into the RETA system thermal-hydraulics code framework[10], which provides fundamental capabilities like nonlinear equation solvers, component design, physical module design, and IOs. A HeatPipe component and the associated discretization objects are added to achieve the previously described heat pipe models, as shown in Fig. 2.

The governing equations for heat pipes are discretized using the Finite Volume Method (FVM) on structured, orthogonal grids. The Backward Discretization Formula is employed for the transient terms. Following the temporal and spatial discretization, a set of coupled Nonlinear Algebraic Equations (NAEs) is generated. Nonlinearity is unavoidable and will be resolved iteratively using a Newton-type nonlinear equation solver.
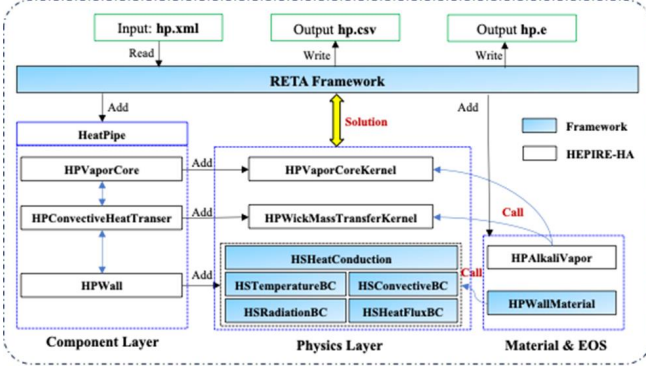

Fig. 2. The structure of the heat pipe analysis code HePIRE-HA.

Let $\mathbf{x}$ be the unknown solution and $\mathbf{R}$ be the residual vector of the system of NAEs:

$$\mathbf{R}(\mathbf{x}) = \mathbf{0} \tag{19}$$

The Newton's method (with a line search algorithm) solves the system of NAEs iteratively by:

$$\mathbb{J}(\mathbf{x}_k) \cdot \delta\mathbf{x} = -\mathbf{R}(\mathbf{x}_k) \tag{20}$$

$$\mathbf{x}_{k+1} = \mathbf{x}_k + \alpha \cdot \delta\mathbf{x} \tag{21}$$

in which k is the nonlinear iteration index, $\mathbb{J}$ is the system Jacobian matrix, and α is the line search relaxation factor. Equation (20) can be solved with either a direct or an iterative linear equation solver. A Preconditioned Jacobian-Free Newton-Krylov (PJFNK) solver is developed to reduce the burden of calculating the exact Jacobian matrix. In the PJFNK method, Equation (20) is replaced by

$$\mathbb{A} \cdot \mathbf{y} = -\mathbf{R}(\mathbf{x}_k) \tag{22}$$

$$\mathbb{A} \equiv \mathbb{D}(\mathbf{x}_k) \cdot \mathbb{P}^{-1}, \mathbf{y} \equiv \mathbb{P} \cdot \delta\mathbf{x} \tag{23}$$

in which $\mathbb{A}$ is the right-preconditioned Jacobian matrix and $\mathbb{P}$ is the preconditioning matrix. In the PJFNK method, Equation (22) is solved with a Krylov subspace solver. To address convergence issues, an automatic time step size adjustment algorithm is included in the solver. If the nonlinear solver fails to converge, the time step size is reduced by half. This approach is vital to enhance the solver's robustness during long-term simulations.

D. Coupling interface

This work considers modeling the reactor core with the ANSYS/Fluent software[32]. A coupling interface is created with the UDF module from ANSYS. The reactor core and heat pipes are coupled at the outer surface of the heat pipe evaporator via convective heat transfer. As described in the previous section, the heat pipe is modeled with an axisymmetric 2D model. The dimension mismatch at the coupling boundaries, i.e., 2D and 1D in the reactor core and heat pipe, is the main difficulty in designing the coupling interface. As shown in Fig. 3, a pseudo fluid with no heat capacity is added to facilitate the coupling and data exchange between the reactor core and heat pipes. The boundary involves the exchange of heat flux and the wall surface temperature of the heat pipe evaporator. Users can specify an equivalent heat transfer coefficient to indicate the thermal resistance between the reactor core and the heat pipe wall.
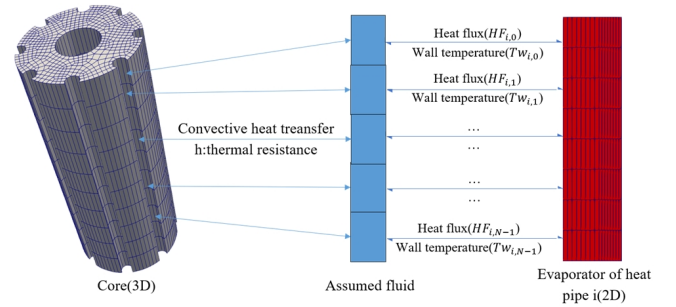
Fig. 3. Schematic of the coupling interface between ANSYS/Fluent and HePIRE-HA.

In the ANSYS reactor core model, a convective boundary condition is set at the coupling boundary by utilizing the temperature of the heat pipe wall surface. The heat flux at this boundary is calculated and then relayed to the heat pipe model. In the HePIRE-HA heat pipe model, a heat flux boundary condition is applied at the coupling boundary, and the heat pipe surface temperature is computed and transferred to the reactor core model. The operator splitting technique facilitates iterations between the core model and the heat pipe model.

III. MODEL VERIFICATION AND VALIDATION

A series of tests for verification and validation are performed to evaluate the reliability and accuracy of both the heat pipe model and the coupling model. A validation study for the heat pipe model includes a steady-state operation test and a transient frozen startup test, utilizing experimental data from the literature. For verification of the coupling model, a cylindrical fuel cell is made up and simulated with the coupled model. The physical conditions for this fuel cell test are quite simple, such that an analytical solution can be derived for verification purposes. The convergence behavior of the coupling model will also be assessed with this fuel cell test.

A. Heat pipe steady-state model validation

In this subsection, we will conduct two steady-state validation studies using experimental data and reference results from other codes available in the literature. The validation cases are based on cylindrical sodium heat pipe experiments conducted by Ivanovskii[33], where vapor temperatures were measured and reported. In addition to the experimental data, simulation results from Chen and Faghri[34] are also used as reference results for a code-to-code comparison, which includes results from a compressible model.

Two cylindrical sodium heat pipes are modeled. The details of physical and boundary conditions are listed in Table 2. $k_{s,wick}$ and $k_{s,wall}$ represents the thermal conductivity of the wick and wall; L_e, L_a, and L_c are the length of evaporation, adiabatic, and condensation region in the axial direction; δ_{wall} and δ_{wick} represent the thickness of the wick and wall in the radial direction; R_v is the radius of the vapor core; Q represents the total heating power applied to the evaporator section; h_{sink} and T_{sink} represent the convective heat transfer coefficient and the coolant temperature in condensation outer wall.

Fig. 4(a) and Fig. 4(b) show the comparison between numerical results from this study and reference results, including both experiment data and simulation results from the literature. Results show that the prediction of vapor temperature by HePIRE-HA matches the experimental data wall. When $Q = 560$ W, the average relative error of the HePIRE-HA simulation results is 0.2%, with a maximum temperature deviation of 4 K near the evaporator-adiabatic interface. There is a vapor temperature drop of 12 K from the evaporator end to the condenser end. A similar trend is found when compared with the reference simulation results. When $Q = 1000$ W, the vapor temperature drop from the evaporator end to the condenser end is about 8 K, which is smaller than the $Q = 560$ W case. This is reasonable because the heat pipe vapor temperature and vapor density are higher in the Q = 1000 W case, and the effective thermal conductivity of the heat pipe is larger. These two test cases were run in the steady-state mode, i.e., the numerical solver found the results in one step from an arbitrary initial condition. The average computation time on an Intel i7 4450H CPU is about 0.22 s, which is quite efficient.

Table 2. Physical and boundary conditions for the heat pipe steady-state validation test cases.

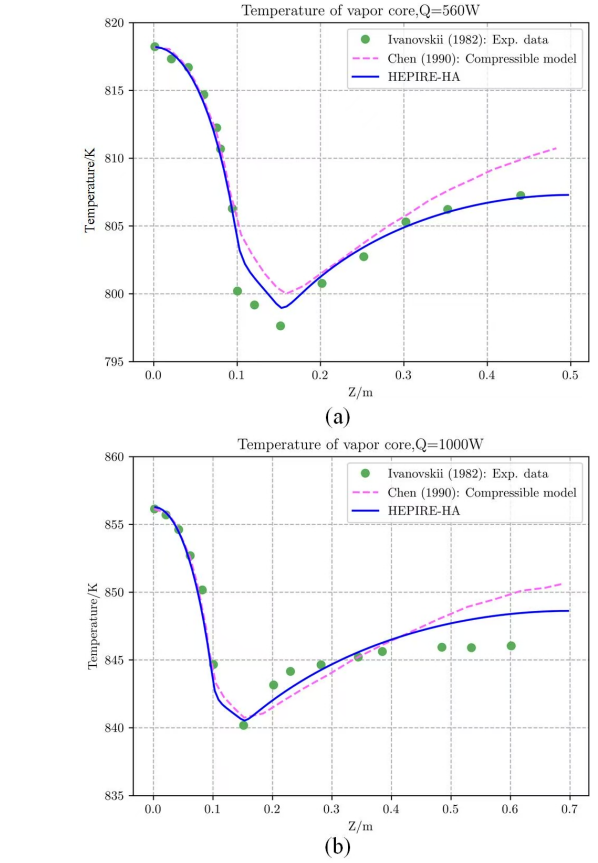| Parameters	Case 1	Case 2
Fluid	Sodium	Sodium
P_c : Pa	1300	2476
T_c : K	818	856
$k_{s,wall}$: W/m · K	19.0	19.0
$k_{s,wic}$: W/m · K	66.2	66.2
R_v : m	0.007	0.007
δ_{wick} : m	0.001	0.001
δ_{wall} : m	0.005	0.005
h_v : W/m^2 · K	1.0E+6	1.0E+6
Q : W	560	1000
h_{sink} : W/m^2 · K	59.6	62.6
T_{sink} : K	300	300
Number of axial elements	80	112

(a)

(b)

Fig. 4. The axial vapor temperature profile for the sodium heat pipe with $Q = 560$ W, (b)The axial vapor temperature profile for the sodium heat pipe with $Q = 1000$ W.

B. Heat pipe startup model validation

Following the steady-state operation validation study, a transient frozen startup validation study was conducted using the cylindrical sodium heat pipe experiments conducted by Faghri and co-authors[35]. Besides the experimental data, simulation results from Yoo[6] are also used as reference re-

sults for a code-to-code comparison. In Yoo's simulation model, a thermal resistance network was constructed based on the frozen startup model. The physical and boundary conditions for this test case are listed in Table 3.

In this experiment test, the heat pipe wall temperature at several axial spots was measured at different times. The heat pipe started with a cold temperature of 300 K and took heat from the resistance heaters. To account for the additional heat capacities of the resistance heaters and radiation shields, an estimated heat capacity of $3.75 \times 10^6 \, \mathrm{J/\left(m^3 \cdot K\right)}$ is added to the heat pipe wall.

Table 3. Physical and boundary conditions for the heat pipe frozen startup test.

Parameters	value	Parameters	value
L_e : (mm)	93.0	Fluid	Sodium
L_a : (mm)	188.0	Wick material	SS304
L_c : (mm)	500.0	Wall material	SS304
R_v : mm	10.75	Porosity	0.7
δ_{wick} : mm	0.5	Emissivity	0.645
δ_{wall} : mm	1.0	Power: W	112
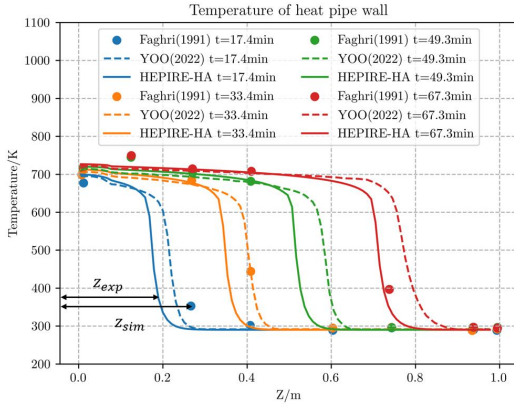
Fig. 5. Comparison of heat pipe wall temperature profile for the frozen startup test.

As shown in Fig. 5, from 17.4 minutes to 67.3 minutes, as heat flux was applied to the heat pipe evaporator wall, the thermal front gradually moved towards the condenser. the prediction of wall temperature during the transient by HePIRE-HA matches the experiment data reasonably well but shows a non-negligible discrepancy in capturing the frozen interface, which indicates that the current treatment of the vapor flow under different conditions may need further improvement. Note that the reference simulation results showed similar discrepancies in predicting the frozen interface. In the current model, the condition of vapor flow is determined by the transition temperatures, which are fixed values determined by the vapor core diameter and transition Kn number. The code determines the interface between different vapor states by the transition temperature and gives a sharp discontinuity across the interface. In reality, the frozen interface is much smoother along the axial direction.

C. Coupling model verification

A made-up fuel cell consists of a cylindrical fuel region and a central heat pipe is used to verify the coupling model. The schematic of this fuel cell is shown in Fig. 6(a). The fuel region is a cylindrical shell with an inner and outer radius of 0.5 m and 1.0 m, respectively. The fuel inner surface is coupled to a cylindrical heat pipe evaporator surface; a fixed temperature (T_{out}) is applied at the fuel outer surface. A convective boundary condition is applied at the heat pipe condenser surface with a fixed ambient heat transfer coefficient (h_{amb}) and ambient temperature (T_{amb}). A constant thermal conductivity is used for the fuel region (k_{fuel}) and heat pipe wall (k_{HP}). Detailed physical and boundary conditions are listed in Table 4.

Table 4. Physical and boundary conditions for the fuel cell verification test.

Parameters	value	Parameters	value
L_e : mm	400.0	H : mm	400.0
L_a : mm	400.0	k_{HP} : W/$\left(m^2 \cdot K\right)$	30.0
L_c : mm	200.0	k_{fuel} : W/$\left(m^2 \cdot K\right)$	0.2
R_v : mm	10.0	T_{out} : K	1009.9
δ_{wick} : mm	0.5	h_{amb} : W/$\left(m \cdot K\right)$	20.0
δ_{wall} : mm	1.5	T_{amb} : K	650.0

For this test case, the temperature distribution in the fuel cell can be derived analytically by assuming that the temperature drop across the heat pipe vapor core is negligible, i.e. the total thermal resistance of the heat pipe is mainly determined by the thermal resistance of the heat pipe wall.

Though this is a very simple test condition, it is useful for verifying the coupling model. Fig. 6(b) shows the comparison of radial fuel temperature distribution from code prediction and the analytical result. The agreement is excellent with negligible discrepancy, the relative error between the analytical result and the simulated result is less than 0.1%.

Besides the simulation results, the convergence of the coupling model is another importance key factor to assess. In this test, the convergence history of the total heat flow and the heat pipe evaporator wall temperature is recorded and presented in Fig. 6(c) and Fig. 6(d). It is observed that the coupling model is convergent. In terms of the convergence rate, it takes about 50 iterations to reduce the relative error by 2 order of magnitude. This convergence rate is not excellent and this is an area for future improvement.

IV. DEMONSTRATION

A heat pipe cooled reactor unit is selected to demonstrate and assess the performance of the previously developed coupling model. The KRUSTY reactor[27] is a demonstration reactor for the design, development, and testing of kilowatt-level reactors. The KRUSTY reactor has a rated thermal power of 5 kW and generates 1 kW of electric power through a Stirling energy conversion device. The reactivity is controlled by a moving axial reflector and a central control rod.
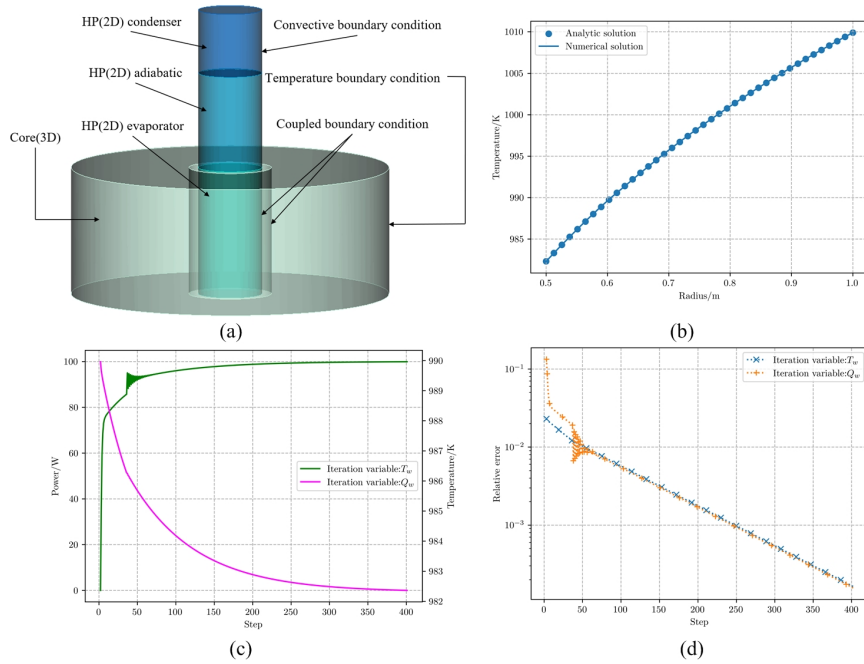
Fig. 6. (a) Schematic of the made-up fuel cell, (b) Radial temperature distribution in the fuel cell predicted by the coupling model, (c) Radial temperature distribution in the fuel cell predicted by the coupling model, (d) Convergence history of iteration variables.

The schematic diagram of the reactor is shown in Fig. 7(a). The clamp provides clamping force to ensure close contact between the heat pipe and the fuel. The heat pipe wall material is Haynes 230 alloy. Up to now, several tests and experiments such as steady-state operation, load following, and startup have been conducted on the KRUSTY reactor. A load following test[36] of the KRUSTY reactor program is selected to demonstrate and validate the newly developed coupling model. This study is conducted in two steps.

In the first step, the steady-state operation of the reactor is simulated. The reactor core is modeled by ANSYS with the volumetric heating power density calculated by the OpenMC software[37]. For the steady-state operation, the total reactor power is 2678 W. The heat pipes are modeled by the HePIRE-HA code. The temperature at the heat pipe condenser outer wall surface is set at 1064 K. The Temperature and Mach number of vapor flow for the heat pipe is shown in Fig. 7(c). The maximum of Mach number of vapor flow is 0.016, and the mean temperature of the heat pipe evaporator outer wall is 1066.9 K, meaning that there is a temperature rise of 2.9K from the heat pipe condenser outer wall to the evaporator outer wall. The fuel temperature distribution is the main quantity of interest and is shown in Fig. 7(b). The maximum fuel temperature is about 1082.5 K, meaning that there is a temperature drop of 17.5 K from the fuel center to the heat pipe condenser outer wall. This reflects the excellent heat transport capability of the heat pipes. However, since the thermal resistance between the fuel and heat pipe wall is not considered, the realistic temperature drop could be higher.

In the second step, a load following transient is simulated by restarting from the steady-state simulation. At the start of this transient process, it is assumed that the external load has dropped by 20%, meaning that the total heat removed by the heat pipes dropped suddenly from the steady-state 2678 W to 2117 W.

The reactivity feedback from fuel temperature change must be modeled to simulate accurately this load following transient. The point kinetics equation model from the RETA code is used to predict the transient reactor power. In this study, the reactivity feedback due to fuel temperature change and Sodium redistribution in the heat pipes are considered. In this study, the fuel temperature reactivity coefficient and reactor power reactivity coefficient are calculated by Postan[36], and the fuel temperature reactivity coefficient is -0.2825 cents/K. The Sodium redistribution is mainly affected by the input power in the evaporator of heat pipes; a reactor power reactivity coefficient of -0.0015 cents/W is used.

This transient simulation is performed using the coupling model, and the results are shown in Fig. 7(d). The reactor power, average fuel temperature, and total reactivity during the transient are presented. At time 0s, due to the sudden drop in external load, the total heat removed by heat pipes drops while the reactor power remains unaffected. This results in a short-term increase in fuel temperature. Then, the reactor power drops due to the negative fuel temperature reactivity feedback. After the reactor power drops to a certain level, the reactor power starts to increase again due to the Sodium redistribution effect. The combination of fuel temperature and Sodium redistribution reactive feedback causes oscillations in both the reactor power and the fuel temperature. After about 2000s following the start of this transient, the reactor power stabilized to a lower level consistent with the external load power 2.17kW, the average fuel increased about 3K. In this way, positive reactivity caused by fuel temperature in-
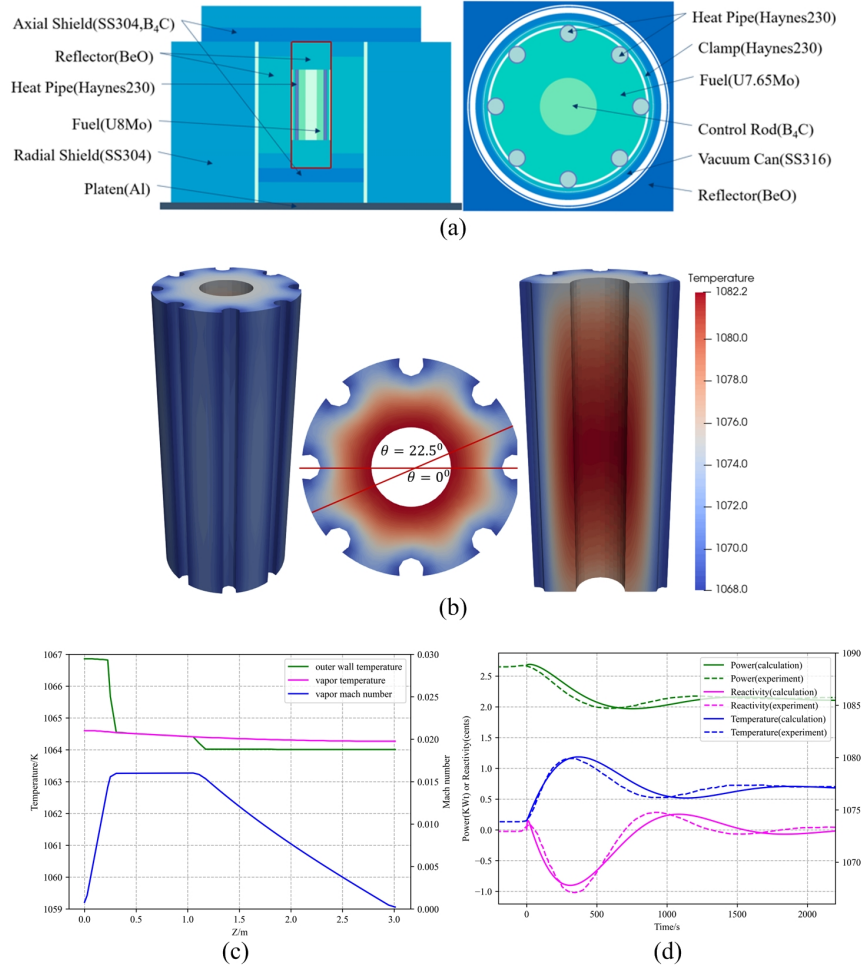
Fig. 7. (a) Schematic of the KRUSTY heat pipe reactor, (b) Steady-state fuel temperature distribution, (c) the axial temperature and Mach number for the sodium heat pipe, (d) Profile of reactor power, average fuel temperature, and total reactivity during the load following transient.

crease is equal to negative reactivity caused by reactor power decrease. It is observed that the prediction by the coupling model matches the experimental data reasonably well. However, there is a visible discrepancy between the model prediction and experimental data. The uncertainty in the predictions could be large due to assumptions and simplifications made when developing this new model, e.g.,Assumptions of the Point Reactor Kinetics Equations, simplification of the reactor core geometry, idealized boundary conditions at the heat pipe condenser surface, etc.

V. CONCLUSION AND FUTURE WORK

To conclude, this work develops an efficient high-temperature alkali metal heat pipe analysis code (HePIRE-HA). HePIRE-HA leverages the highly flexible code structure and highly efficient numerical solution schemes of the RETA advanced system analysis software. A compressible two-equation model for the heat pipe vapor core is developed, which is capable of simulating both steady-state operation and transient startup of the heat pipes. A validation study with both steady-state and frozen startup experiment data shows that the HePIRE-HA code is accurate and robust enough to handle the complex behaviors happening inside heat pipes. The computation efficiency of the HePIRE-HA code is excellent, making it quite suitable for long-time transient simulations as commonly required by reactor design and safety analysis studies.

In addition to the standalone heat pipe analysis software, a coupling interface is developed using the ANSYS UDF module to model and simulate the HP MicroRx reactor core. Using a pseudo fluid with zero heat capacity, the coupling interface successfully resolves the issues caused by the mismatch in the dimensions at the coupling boundary. The coupling model is verified by studying a made-up fuel cell test case and validated by the KRUSTY load following test.

Results from the V&V and demonstration studies show that the heat pipe analysis model is reliable, robust, and efficient. However, results also show that the current heat pipe analysis model needs further improvement to capture more accurately the frozen startup boundary in the vapor core by using more accurate Rarefied vapor flow model. The convergence rate of the current coupling model could be significantly improved

to accelerate the computation of the reactor core analysis by using relaxed picard iteration.

[1] H. Gu, Z. Shouzhi, Overview of space nuclear reactor power technology. Journal of Deep Space Exploration 4, 5 (2017). https://doi.org/10.15982/j.issn.2095-7777.2017.05.004.

[2] Z. Anwen, L. Lei, M. Shijun, et al., An overview of the use and development of nuclear power system in deep space exploration. Journal of Deep Space Exploration 4, 5 (2017). https://doi.org/10.15982/j.issn.2095-7777.2017.05.001.

[3] H. Yu, Z. Zhang, X. Chai, et al., Initiation and development of heat pipe cooled reactor. Nuclear Power Engineering 40, 4 (2019). https://doi.org/10.13832/j.jnpe.2019.04.0001.

[4] A. Faghri, Review and advances in heat pipe science and technology. J. Heat Transfer 134, 12 (2012). https://doi.org/10.1115/1.4007407.

[5] B. Zohuri, Heat pipe design and technology: Modern applications for practical thermal management. (Springer2016).

[6] J. S. Yoo, M. Song, S. Qin, et al., A conduction-based heat pipe model for analyzing the entire process of liquid-metal heat pipe startup. Tech. rep., Idaho National Lab.(INL), Idaho Falls, ID (United States), (2022). https://www.osti.gov/biblio/1856343.

[7] J. E. Hansel, C. d. S. B. Dutra, L. Charlot, et al., The liquid-conduction, vapor-flow heat pipe model in Sockeye. Nucl. Eng. Des. 426 (2024). https://doi.org/10.1016/j.nucengdes.2024.113359.

[8] J. E. Hansel, R. A. Berry, D. Andrs, et al., Sockeye: A one-dimensional, two-phase, compressible flow heat pipe application. Nucl. Technol. 207, 7 (2021). https://doi.org/10.1080/00295450.2020.1861879.

[9] G. Hu, Development of Heat Pipe Modeling Capabilities in a Fully-Implicit Solution Framework. International Confernece Pacific Basin Nuclear Conference, (Springer, 2022). https://doi.org/10.1007/978-981-99-1023-6_72.

[10] G. Hu, Development of a Fully-Implicit Second-Order system Thermal-Hydraulics analysis code for reactor modeling and simulations. Nucl. Eng. Des. 415 (2023). https://doi.org/10.1016/j.nucengdes.2023.112715.

[11] C. Mueller, P. Tsvetkov, A review of heat-pipe modeling and simulation approaches in nuclear systems design and analysis. Ann. Nucl. Energy 160 (2021). https://doi.org/10.1016/j.anucene.2021.108393.

[12] Y. Ma, J. Liu, H. Yu, et al., Coupled irradiation-thermal-mechanical analysis of the solid-state core in a heat pipe cooled reactor. Nucl. Eng. Technol. 54, 6 (2022). https://doi.org/10.1016/j.net.2022.01.002.

[13] Z. Zhang, C. Wang, K. Guo, et al., HEART, a specific code for thermal-electrical analysis of heat pipe cooled nuclear reactor. Int. J. Therm. Sci. 179 (2022). https://doi.org/10.1016/j.ijthermalsci.2022.107666.

[14] C. Wang, H. Sun, S. Tang, et al., Thermal-hydraulic analysis of a new conceptual heat pipe cooled small nuclear reactor system. Nucl. Eng. Technol. 52, 1 (2020). https://doi.org/10.1016/j.net.2019.06.021.

[15] L. M. Alawneh, R. Vaghetto, Y. Hassan, et al., Conceptual design of a 3 MWth yttrium hydride moderated heat pipe cooled micro reactor. Nucl. Eng. Des. 397 (2022). https://doi.org/10.1016/j.nucengdes.2022.111931.

[16] L. Ge, H. Li, X. Tian, et al., Improvement and validation of the system analysis model and code for heat-pipe-cooled microreactor. Energies 15 , 7 (2022. https://doi.org/10.3390/en15072586.)

[17] C. Wang, H. Sun, S. Tang, et al., Thermal-hydraulic analysis of a new conceptual heat pipe cooled small nuclear reactor system. Nucl. Eng. Technol. 52, 1 (2020). https://doi.org/10.1016/j.net.2019.06.021.

[18] Z. Zhang, C. Wang, K. Guo, et al., HEART, a specific code for thermal-electrical analysis of heat pipe cooled nuclear reactor. Int. J. Therm. Sci. 179 (2022). https://doi.org/10.1016/j.ijthermalsci.2022.107666.

[19] Y. Ma, C. Tian, H. Yu, et al., Transient heat pipe failure accident analysis of a megawatt heat pipe cooled reactor. Prog. Nucl. Energy 140 (2021). https://doi.org/10.1016/j.pnucene.2021.103904.

[20] Y. Ma, C. Tian, H. Yu, et al., Transient heat pipe failure accident analysis of a megawatt heat pipe cooled reactor. Prog. Nucl. Energy 140 (2021). https://doi.org/10.1016/j.pnucene.2021.103904.

[21] G. Hu, R. Hu, J. Kelly, et al., Multi-physics simulations of heat pipe micro reactor. Tech. rep., Argonne National Lab.(ANL), Argonne, IL (United States), 2019, https://doi.org/10.2172/1569948.

[22] C. Matthews, V. Laboure, M. DeHart, et al., Coupled multiphysics simulations of heat pipe microreactors using DireWolf. Nucl. Technol. 207, 7 (2021). https://doi.org/10.1080/00295450.2021.1906474.

[23] Y. Yuan, J. Shan, B. Zhang, et al., Accident analysis of heat pipe cooled and AMTEC conversion space reactor system. Ann. Nucl. Energy 94 (2016). https://doi.org/10.1016/j.anucene.2016.04.017.

[24] Z. Zhipeng, Y. Haoran, W. Haiping, et al., Neutronics and Thermal-hydraulics Analysis of Megawatt-class Level Heat Pipe Reactor. Atomic Energy Science and Technology 56, 9 (2022). https://doi.org/10.7538/yzk.2021.youxian.0712.

[25] Y. Guo, Z. Li, K. Wang, et al., A transient multiphysics coupling method based on OpenFOAM for heat pipe cooled reactors. Sci. China Technol. Sci. 65 , 1 (2022). https://doi.org/10.1007/s11431-021-1874-0.

[26] C. Lee, Y. S. Jung, Development of the PROTEUS and ANSYS coupled system for simulating heat pipe cooled micro reactors. Tech. rep., Argonne National Lab.(ANL), Argonne, IL (United States, 2020). https://doi.org/10.2172/1601796.

[27] D. I. Poston, M. A. Gibson, T. Godfroy, et al., KRUSTY reactor design. Nucl. Technol. 206, sup1 (2020). https://doi.org/10.1080/00295450.2020.1725382.

[28] J. H. Jang, A. Faghri, W. S. Chang, et al., Mathematical modeling and analysis of heat pipe start-up from the frozen state. ASME. J. Heat Transfer. 112, 3 (1990). https://doi.org/10.1115/1.2910427.

[29] D. K. Edwards, V. E. Denny, A. F. Mills, Transfer processes. an introduction to diffusion, convection and radiation, Series in Thermal and Fluids Engineering (1978).

[30] J. K. Fink and L. Leibowitz, Thermodynamic and transport properties of sodium liquid and vapor, Report (1995). https://doi.org/10.2172/94649

[31] H. H. Coe, Summary of thermophysical properties of potassium, Report (1965).

[32] J. E. Matsson, An introduction to ansys fluent 2023, (Sdc Publications, 2023).

[33] M. Ivanovski, V. P. Sorokin, I. V. Yagodkin, Physical principles of heat pipes. (1982). https://www.osti.gov/biblio/6148667.

[34] M.-M. Chen, A. Faghri, An analysis of the vapor flow and the heat conduction through the liquid-wick and pipe wall in a heat pipe with single or multiple heat sources. Int. J. Heat Mass Transfer 33, 9 (1990). https://doi.org/10.1016/0017-9310(90)90226-K.

[35] A. Faghri, M. Buchko, Y. Cao, A study of high-temperature heat pipes with multiple heat sources and sinks: Part I—Experimental methodology and frozen startup profiles. 113, 4 (1991). https://doi.org/10.1115/1.2911193.

[36] D. I. Poston, Space Nuclear Reactor Engineering, Tech. rep., Los Alamos National Laboratory (LANL). Los Alamos, NM (United States, 2017). https://doi.org/10.2172/1345963.

[37] P. K. Romano, B. Forget, The OpenMC monte carlo particle transport code. Ann. Nucl. Energy 51 (2013). https://doi.org/10.1016/j.anucene.2012.06.040.